Wetlands of North Africa During the Mid-Holocene were At Least Five Times the Area Today

Weizhe Chen, Philippe Ciais, Chunjing Qiu, Agnès Ducharne, Dan Zhu, Shushi Peng, Pascale Braconnot, Chunju Huang

▶ **To cite this version:**

Weizhe Chen, Philippe Ciais, Chunjing Qiu, Agnès Ducharne, Dan Zhu, et al.. Wetlands of North Africa During the Mid-Holocene were At Least Five Times the Area Today. Geophysical Research Letters, American Geophysical Union, 2021, 10.1029/2021GL094194 . hal-03373303

HAL Id: hal-03373303

https://hal.archives-ouvertes.fr/hal-03373303

Submitted on 19 Aug 2022

HAL is a multi-disciplinary open access archive for the deposit and dissemination of scientific research documents, whether they are published or not. The documents may come from teaching and research institutions in France or abroad, or from public or private research centers.

L'archive ouverte pluridisciplinaire **HAL**, est destinée au dépôt et à la diffusion de documents scientifiques de niveau recherche, publiés ou non, émanant des établissements d'enseignement et de recherche français ou étrangers, des laboratoires publics ou privés.

Copyright

Check for updates

AGU ADVANCING EARTH AND SPACE SCIENCE

Geophysical Research Letters®

RESEARCH LETTER
10.1029/2021GL094194

Key Points:

- We present high-resolution reconstructions of wetland distribution up to 15″ for the mid-Holocene North Africa
- During the mid-Holocene, 18.9 ± 4.0% of land surface in North Africa was covered by wetlands
- The relationship between precipitation and wetland fraction in the mid-Holocene Sahara is explored

Supporting Information:

Supporting Information may be found in the online version of this article.

Correspondence to:

W. Chen and C. Qiu,
wzchen@cug.edu.cn;
chunjing.qiu@lsce.ipsl.fr

Citation:

Chen, W., Ciais, P., Qiu, C., Ducharne, A., Zhu, D., Peng, S., et al. (2021). Wetlands of North Africa during the mid-Holocene were at least five times the area today. *Geophysical Research Letters*, *48*, e2021GL094194. https://doi.org/10.1029/2021GL094194

Received 5 MAY 2021
Accepted 1 OCT 2021

© 2021. American Geophysical Union. All Rights Reserved.

Wetlands of North Africa During the Mid-Holocene Were at Least Five Times the Area Today

Weizhe Chen[1,2], Philippe Ciais[2,3], Chunjing Qiu[2], Agnès Ducharne[4], Dan Zhu[5], Shushi Peng[5], Pascale Braconnot[2], and Chunju Huang[1]

[1]State Key Laboratory of Biogeology and Environmental Geology, Hubei Key Laboratory of Critical Zone Evolution, School of Earth Sciences, China University of Geosciences, Wuhan, China, [2]Laboratoire des Sciences du Climat et de l'Environnement, LSCE/IPSL, CEA-CNRS-UVSQ, Université Paris-Saclay, Gif-sur-Yvette, France, [3]Climate and Atmosphere Research Center (CARE-C), The Cyprus Institute (CyI), Nicosia, Cyprus, [4]Laboratory METIS (Milieux Environnementaux, Transferts et Interaction dans les hydrosystèmes et les Sols), CNRS, EPHE, Sorbonne Université, Paris, France, [5]Sino-French Institute for Earth System Science, College of Urban and Environmental Sciences, Peking University, Beijing, China

Abstract The Sahara was significantly wetter and greener than today during the mid-Holocene (~6,000 years before present), and those conditions were likely maintained by feedbacks from evaporating wetlands and riparian zones. A lack of spatially continuous wetland reconstruction is the major obstacle to investigating their impacts on climate and vegetation during that epoch. Here, we estimate high-resolution gridded wetland distribution up to 15″ in the mid-Holocene North Africa obtained with three statistical and hydrological modeling approaches forced by enhanced and calibrated precipitation from climate models. These wetland models have good performance for present-day conditions and reproduce mid-Holocene hydrological elements evaluated by 297 paleo-records. Simulation results show that 18.9 ± 4.0% of land surface in North Africa was covered by wetlands during the mid-Holocene. Our results highlight the impact of natural climate change on wetland areas and provide a data set for modeling studies to include wetland feedbacks.

Plain Language Summary Several lines of evidence show that northern Africa was considerably wetter and greener than today at ~6,000 years ago, which is known as the mid-Holocene Green Sahara (GS). However, most current models could not reproduce climate in the GS. The importance of wetland feedbacks on sustaining a wetter climate has partially been recognized while large uncertainties in wetland coverage make it difficult to examine wetland feedbacks in climate models. We trained several wetland models under present climate and applied them to wetland reconstructions of GS. The produced wetland maps could capture dense wetlands indicated by 297 paleo-records. The total wetland fraction in the mid-Holocene North Africa is 18.9 ± 4.0%, which is more than five times the area today (~2.8%). The relationship between wetland fraction and precipitation is examined in our models. This work improves our understanding of the GS enigma, and has implications for potential greening and wetting of Sahel and Sahara in the future.

1. Introduction

The hyperarid Sahara in North Africa is currently the largest hot desert and one of the largest sources of airborne dust on the Earth (Palchan & Torfstein, 2019). But during the early to middle Holocene (11–5 ka), large parts of the Sahara were much wetter and greener than today (Pausata et al., 2020). Evidence for this mid-Holocene "Green Sahara" comes from paleolake deposits (Kropelin et al., 2008; Lézine et al., 2011), river systems (Skonieczny et al., 2015), pollen records (Bartlein et al., 2010), and archaeological findings (Drake et al., 2011; Larrasoana et al., 2013). It is believed that the wetter hydroclimatic conditions experienced by the Sahara were primarily triggered by Earth's orbital cycle (Kutzbach, 1981). However, current state-of-the-art Earth System Models (ESMs) that account for orbital forcing alone cannot reproduce the climate and land cover in the mid-Holocene Green Sahara (Harrison et al., 2015). Despite improvements in the representation of the West African monsoon, the most recent mid-Holocene (6 ka) simulations from Paleoclimate Modelling Intercomparison Project 4 (PMIP4) continue to underestimate the northward extension of West African monsoon (Brierley et al., 2020).

The importance of land-surface and dust feedbacks to maintain a wetter climate in the mid-Holocene Sahara has been recognized (Braconnot et al., 2021; Chandan & Peltier, 2020; Claussen & Gayler, 1997; Texier et al., 2000). For example, ESM simulations showed that Saharan vegetation cover and dust reduction could significantly increase African monsoon precipitation (Sun et al., 2019). Krinner et al. (2012) suggested that open-water surfaces in the Sahara were a strong local moisture source and had effect on the mid-Holocene North Africa climate. However, there are still large uncertainties in land cover reconstructions of wetland coverage due to spatially discontinuous paleo-records (Engel et al., 2017; Quade et al., 2018). This limitation prevents us from quantifying mid-Holocene wetland feedbacks on vegetation (Chen et al., 2020; Tian et al., 2017) and climate (Chandan & Peltier, 2020; Krinner et al., 2012). We argue that a robust reconstruction of wetland distribution is fundamental for a better climate modeling during that period.

Despite the widely recognized importance of wetlands, their definition is inconsistent in the literature (Hu, Niu, & Chen, 2017). In this study, we focused on potential wetlands (including lake areas), which are defined as persistently saturated or near-saturated areas that are regularly subject to inundation or shallow water tables if there were no human disturbance (Tootchi et al., 2019). According to tropical and subtropical wetland areas estimated through combining expert rules and multiple hydrological models and data sets (Gumbricht et al., 2017), only ~0.8% of land surface area in North Africa between 10° and 30°N is currently covered by wetlands. In comparison, estimates from Hoelzmann et al. (1998) suggest that wetlands occupied at least 7.4% of the land surface in the same domain during the mid-Holocene, and they admit it is an underestimate because of limited wetland information for North Africa. Combining digital topographic data, satellite images, and previous studies, Drake et al. (2011) developed a map describing palaeohydrological elements of the mid-Holocene Sahara. Nevertheless, still under debate is the size of some large lakes and the associated rainfall rate (Engel et al., 2017; Quade et al., 2018), let alone wetland areas. Several methods were applied to establish present-day wetland distribution data sets, including remote sensing images classification, aggregation and compilation method, and model simulation (Hu, Niu, & Chen, 2017; Stocker et al., 2014; Xue et al., 2018). The idea of these statistical and hydrological models inspired us to generate the first high-resolution reconstruction of wetlands for the Green Sahara.

This study aims to reconstruct wetland distributions in the mid-Holocene North Africa based on three statistical and process-based approaches. First, these models are trained under the present climate to reproduce present potential wetlands. The mid-Holocene climate variables are calibrated and used to force these wetland models to simulate mid-Holocene wetlands, which are then evaluated against hydrological elements from paleo-records. Final, we determine the most plausible wetland map and explore the relationship between wetland areas and precipitation levels.

2. Materials and Methods

2.1. Predictive Models for Wetland Distribution

Three approaches were used to predict the wetland fraction at mid-Holocene: a simple diagnostic model based on the topography-climate wetness index (TCI), a multivariate random forest model (RFM), and the physically based land surface model ORCHIDEE-PEAT (LSM) with the TOPMODEL water redistribution model. These models were calibrated/trained using data from present, then applied to the mid-Holocene scenario (see flowchart in Figure S1 in Supporting Information S1).

TOPMODEL is a water redistribution model predicting the saturated fraction of a catchment or grid-cell (Beven & Kirkby, 1979). It combines the mean water table depth of a catchment or grid-cell with higher resolution topographic index (TI):

$$\mathrm{TI} = \ln\left(\frac{a}{\tan(\beta)}\right) \tag{1}$$

where upstream drainage area a informs the potential water input to the pixel while local slope $\tan(\beta)$ is a proxy of the propensity to discharge water downstream. Therefore, high values of the TI define a high potential to saturation (Curie et al., 2007).

The first approach (TCI) is adapted from the equations proposed by Merot et al. (2003) to diagnose the potential distribution of wetlands. A larger TCI represents a higher possibility to develop wetlands. Here, we used two TCI formulations called TCI1 and TCI2, after Hu, Niu, Chen, Li et al. (2017) and Tootchi et al. (2019), respectively:

$$\mathrm{TCI1} = \ln\left(\frac{a \times P}{\tan(\beta)}\right) = \mathrm{TI} + \ln(P) \tag{2}$$

$$\mathrm{TCI2} = \ln\left(\frac{a \times Pe}{\tan(\beta)}\right) = \mathrm{TI} + \ln(P - \mathrm{PET}) \tag{3}$$

where P is the annual precipitation (mm/yr), and P_e is the mean annual effective precipitation (mm/yr), defined as the difference between precipitation and potential evapotranspiration (PET). The key parameter is the TCI threshold separating wetlands from unsaturated soils for each pixel at 15″. This parameter was calibrated under the present climate to match the composite wetland map of Tootchi et al. (2019).

The second approach (RFM) is a non-parametric random forest (RF) ensemble classifier that produces classification trees from a training data set (Breiman, 2001; Cutler et al., 2007). RF can well handle high-dimensional data and has been widely used for wetland identification (Felton et al., 2019; Xue et al., 2018). In this study, RFM was trained to simulate current wetland distribution at 15″ from eight predictors, including five climate variables (average temperature, precipitation, solar radiation, wind speed, and water vapor pressure), two hydrologic variables (drainage basin and river network), and the topographic variable TI.

The third approach (LSM) is the process-oriented land surface model ORCHIDEE-MICT coupled with the TOPMODEL sub-grid hydrological scheme, namely ORCHIDEE-PEAT (Qiu et al., 2019). It incorporates the cost-efficient version of TOPMODEL proposed by Stocker et al. (2014) to diagnose the wetland fraction (inundated fraction) of each grid-cell from the mean soil moisture simulated by ORCHIDEE-PEAT and the high-resolution TI distribution. The parameters of this TOPMODEL-based approach were calibrated for each 0.5° grid cell to reproduce the present-day wetland fractions and then the ORCHIDEE-PEAT model was forced by mid-Holocene climate fields to simulate mid-Holocene wetland areas. The boundary conditions of the simulation (i.e., soil texture), other than climate forcing and TOPMODEL parameters, are the same as Chen et al. (2020).

2.2. Data Preparation for Models

For present-day, climate data used as input of diagnostic wetland models were downloaded from Global Climate Data (WorldClim V2.1), at a spatial resolution of 30″ (~1 km) (Fick & Hijmans, 2017). Climate variables include 2-m air temperature, precipitation, solar radiation, wind speed, and water vapor pressure. For the pre-industrial (PI) period, we used climate fields from the six-hourly CRUNCEP V8 gridded climate data set at 0.5° spatial resolution during 1901–1910 (Wei et al., 2014).

For mid-Holocene climate, we considered 15 different available ESM simulations (Table S1 in Supporting Information S1): 10 mid-Holocene simulations in PMIP4 (Brierley et al., 2020) and 5 individual climate simulations from other ESMs (Armstrong et al., 2019; Beyer et al., 2020; Chandan & Peltier, 2020; Hijmans et al., 2005; Sun et al., 2019). However, these simulations either significantly underestimated the precipitation or lack other necessary climate variables (Figures S2 and S3 in Supporting Information S1). Thus, we firstly selected precipitation data from two climate models, the IPSL-CM6A-LR (Boucher et al., 2020; Braconnot et al., 2021) to represent PMIP4 and the EC-Earth (Sun et al., 2019) which produced the strongest precipitation over these simulations. After enhancement of precipitation (Figure S4 in Supporting Information S1) and bias-correction (O'ishi & Abe-Ouchi, 2013; Wei et al., 2014), four plausible rainfall maps (MH1–MH4) were produced to cover the error range from the spread of different ESMs (see flowchart in Figure S5 and Text S1 in Supporting Information S1). Other required climate variables were taken and calibrated from the IPSL-CM6A-LR model, assuming that this model could better capture these climate variables than rainfall for mid-Holocene Africa (Brierley et al., 2020).

Besides climate variables, topographic and hydrologic variables were used as predictors. The global map of TI was developed by Marthews et al. (2015) at 15″. The level 1 drainage basin boundary was collected from

GRDC (2020), which was converted to gridded basin number for RFM. The present-day global river network was obtained from HydroRivers (Lehner & Grill, 2013) at 15″, which is a binary map. For the mid-Holocene, we digitized the paleo-hydrological complex of lakes, rivers, and alluvial plains from previous reconstructions in the North Arica (Drake et al., 2011; Larrasoana et al., 2013) in Qgis software and then converted it to 15″ raster data. The present-day wetland map used to train wetland models is one of the 15″ composite maps (CW-TCI15) of Tootchi et al. (2019), which combine regularly flooded wetlands through overlapping open-water and inundation data sets, and groundwater-driven wetlands.

To evaluate model results against independent field-based reconstructions, mid-Holocene lake status data indicated by paleo-records were compiled based on previous studies (Kohfeld & Harrison, 2000; Lézine et al., 2014). A total of 297 paleolake records were selected between 8 and 5 ka in North Africa.

3. Results

3.1. Performance of the Models to Reproduce Present Wetlands

In the reference binary map (Tootchi et al., 2019), present-day potential wetlands occupy 13.7% of land area in North Africa (0°–35°N) (Figure 2a). To evaluate the ability of the TCI and RFM approaches to reproduce the reference binary wetland map at a pixel scale of 15″, receiver operating characteristic (ROC) curve (Swets, 1988) was calculated (Figures 2g and 2h). The area under the curve (AUC) reflects the accuracy of the model.

In the TCI1, the ROC curve gives an AUC value of 0.78, indicating that it is a useful model to reproduce wetland distribution (Figure 2g). Total accuracy (ACC), namely the percentage of true positive plus true negative, is 83% (Table S2 in Supporting Information S1). The TCI1 approach tends to overestimate wetlands in dry regions and underestimate wetlands in wet regions (Figure 2b). After including PET in the TCI2, the predicted wetland has better agreement with the reference wetland distribution (Figure 2c) and results in higher AUC value of 0.82, and ACC value of 84%.

For the RFM1, a random selection of 100,000 pixels (i.e., ~0.11% of land pixels) over the studied region was used as training samples. The model is ranked as useful since AUC is 0.83 and ACC is 88% (Figures 2d and 2h; Table S2 in Supporting Information S1). The produced total wetland fraction of 7.3% is underestimated compared with the reference map. For the alternative model RFM2, training samples are replaced with 100,000 random pixels between 0° and 15°N where wetlands are denser. The predicted total wetland fraction increases to 8.6%.

For the LSM, only reference data between 0° and 10°N were used for calibration, because the lack of wetland north of 10°N today makes it difficult to retrieve practical TOPMODEL parameters. The simulated wetland fraction at 0.5° resolution is evaluated against the reference map (Figure 2i). Because the LSM provides a continuous wetland fraction at coarse resolution (instead of a binary wetland and non-wetland classification like other approaches), we used a regression analysis with the observed fraction at 0.5°. The results show that the correlation coefficient is 0.8 and that the model tends to underestimate wetland fraction. For the mid-Holocene simulation, the median value of TOPMODEL parameters over 0–10°N is extrapolated to regions north of 10°N.

In general, the TCI2 and RFM1 have the best agreement with the reference map at 15″ (Table S2 in Supporting Information S1). For the six wetland complexes denoted in Figure 2a, the RFM2 has the best performance, which reproduces the dense wetlands in South Sudan, Niger River Delta, and Cuvette Centrale (in Congo) very well. Only the RFM1 could reproduce the wetlands in the Nile delta. Lake Chad is predicted in all TCI and RFM. The coarser resolution LSM could capture dense wetland areas in South Sudan and Cuvette Centrale.

3.2. Reconstructed Wetlands During the Mid-Holocene

The five calibrated models were applied to reconstruct wetlands of North Africa during the mid-Holocene using the four precipitation gridded fields MH1–MH4 (see Section 2). We propose two different metrics to evaluate the resulting 20 mid-Holocene wetland maps with the 297 paleolake records (Kohfeld &

Harrison, 2000; Lézine et al., 2014) (Figure 3): the Reproducing Efficiency (RE) and the Relative Accuracy (RA) (Table S3 in Supporting Information S1). RE is the percentage of the 297 records that are correctly represented in a simulated mid-Holocene wetland map within each ~1.3-km grid-cell divided by simulated total wetland fraction. RA describes the ability of a simulation to present a higher wetland fraction around the records (i.e., 0.5° grid-box) than average over surrounding regions (i.e., 5° grid-box). Both metrics show that the simulated wetlands from RFM2 with MH2 or MH3 climate have the best agreement with the paleo-records. Furthermore, all models perform the worst with MH1 among the four precipitation forcings, corresponding to the lowest RE and RA values.

In addition to above quantitative evaluation, we also presented a qualitative comparison between the simulated mid-Holocene wetland fraction at 0.1° and the 297 records (Figure 4a). We found that the higher predicted wetland fraction with the RFM2 approach corresponds to denser paleo-hydrological records in Sahara (15°–35°N) and only "intermediate-level" and "high-level" lakes are found for simulated wetland fractions of 50%–100% (Figure 4a). Thus, we interpret 50%–100% of wetland fraction in our map as corresponding to water bodies like paleolakes and rivers. We confined the timespan to 6.5–5.5 ka and the selected number of records decrease from 297 to 182. This shorter timespan has scarce impact on the relationship between paleo-records and simulated wetlands (Figure S6 in Supporting Information S1). Simulation with the TCI2 and LSM approaches could also capture a positive correlation between modeled wetland fractions and density of paleo-records (Figure S7 in Supporting Information S1). This relationship seems independent from grid-cell resolution within a range of 0.025°–1° (Figure S8 in Supporting Information S1). It suggests the overall good performance of TCI2, RFM2, and LSM to classify drylands and wetlands.

Spatial patterns of simulated mid-Holocene wetlands with MH3 climate from the five models are presented in Figure 3, since MH3 is possibly the most plausible rainfall intensity map in our tests (Section 4). As the TCI1 only relies on topographic information and precipitation, a larger precipitation in mid-Holocene than present-day results in more wetlands in the Sahara. Compared with the TCI1, the TCI2 includes PET and therefore predicts less wetland in dry regions. Dense wetlands along lakes between 0° and 20°N (e.g., Megalake Chad and West Nubian Paleolake) are simulated in both TCI predictions, however. The LSM approach with the MH3 rainfall map clearly differentiates drylands and wetlands and the spatial pattern is comparable to paleo-records (Figure 3e; Table S3 in Supporting Information S1). However, the LSM only simulates local wetlands from sub-grid water redistribution but not the wetlands recharged by floods or rivers, and thus it could not capture many paleolakes in Sahara. The generated map from the RFM2 has the best agreement with paleo-records (Figure 3d). Many paleo-hydrological elements are diagnosed, like Megalake Chad, West Nubian Paleolake, paleolakes in Morocco and wetlands along many river networks (e.g., the Nile, the Niger river, the Senegal River, and the Congo River).

4. Discussion

The spatial pattern of annual precipitation in the mid-Holocene Sahara is still uncertain (Bartlein et al., 2010; Brierley et al., 2020; Hopcroft et al., 2017; Molnar & Rajagopalan, 2020; Tierney et al., 2017). To cover the precipitation uncertainty range in the mid-Holocene Sahara, four precipitation levels were tested (Section 2.1), leading to 20 mid-Holocene simulations with five wetland diagnostic models (Figures 4c and 4d). According to previous precipitation estimates from pollen records and vegetation simulations, ~400 mm/yr of annual precipitation is required to sustain grassland and dry shrubland in regions north of 20°N (Bartlein et al., 2010; Chen et al., 2020). In addition, simulated mid-Holocene wetlands with MH1 have the lowest agreement with the 297 records among the four precipitation forcings (Table S3 in Supporting Information S1). Hence, the MH1 forcing with a mean annual rainfall of 734 mm/yr over North Africa is not compatible with these evidences and should be excluded (Figure 1e). The existence and size of the West Nubian Paleolake (18.5°N/25.5°E) in Sudan pointed to an annual precipitation of 500–900 mm/yr (Hoelzmann et al., 2000). Quade et al. (2018) proposed that the Megalake Chad received a rainfall of ~1,250 mm/yr. Consequently, only the MH2 and MH3 forcings are within this range, and MH4 can be excluded because of overestimation (Figure 1e). The well-defined Megalake Chad is not modeled as a wetland/lake in TCI and RFM with the MH2 rainfall but is correctly reproduced with the wetter MH3 climate (Figure 3 and Figure S9 in Supporting Information S1). Therefore, the MH3 forcing with a mean annual rainfall of 1,207 mm/yr over North Africa appears to be a more plausible rainfall regime.

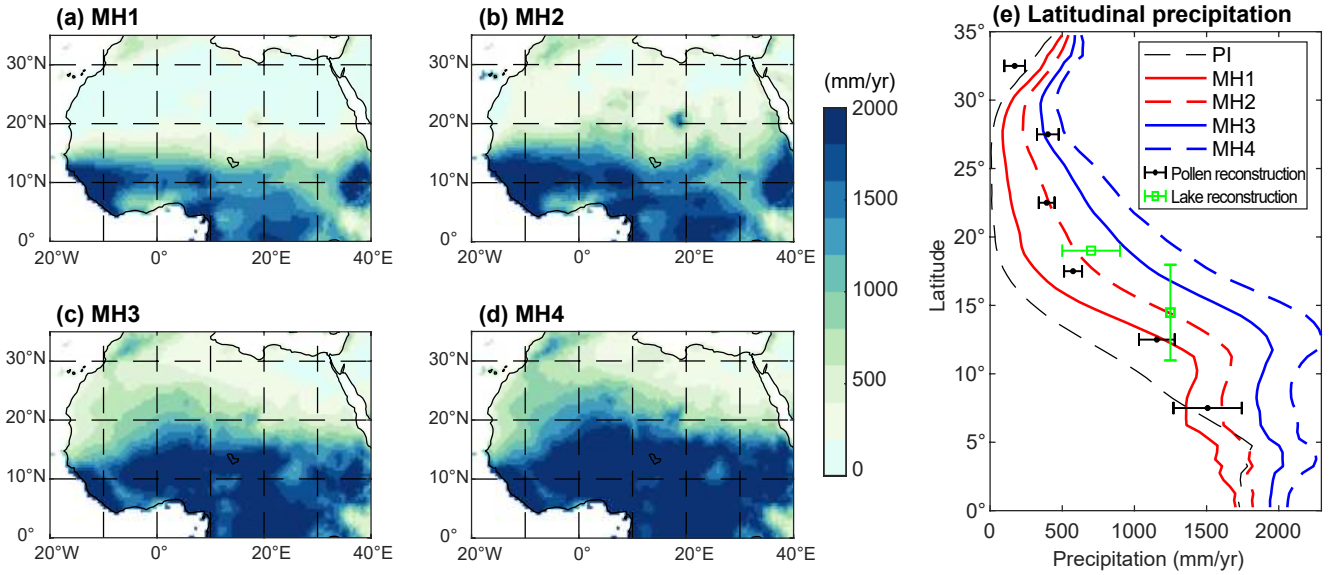

Figure 1. Mean annual precipitation over North Africa. (a and b) The MH1 and MH2 are derived from IPSL-CM6A-LR mid-Holocene simulation (Boucher et al., 2020; Braconnot et al., 2021); (c and d) MH3 and MH4 are based on EC-Earth mid-Holocene simulation (Sun et al., 2019). (e) Latitudinal precipitation comparison between previous reconstructions based on pollen data (Bartlein et al., 2010), the West Nubian Paleolake (18.5°N/25.5°E) in Sudan (Hoelzmann et al., 2000) and the Megalake Chad situated between 10° and 18°N (Quade et al., 2018). Precipitation during the pre-industrial (PI) period is derived from the CRUNCEP V8 gridded climate data set (Wei et al., 2014) during 1901–1910 (Figure S3f in Supporting Information S1).

The simulated total wetland fraction in North Arica was compared with previous reconstructions (Figures 4c and 4d; Table S4 in Supporting Information S1). Previous data set described land-surface conditions in the mid-Holocene North Africa, suggesting that at least 7.4% of the land surface was covered by wetlands between 10° and 30°N (Hoelzmann et al., 1998). An updated map (Drake et al., 2011; Larrasoana et al., 2013) increased this value and suggested that even open water bodies alone occupied ~7% and ~8% of land surface over North Africa and north of 10°N, respectively. Our estimates from five wetland models with the MH2 and MH3 precipitation levels suggest that 18.9 ± 4.0% (mean and standard deviation) of the land surface in North Africa was covered by wetlands, which is at least five times the area today (2.8%) (Figure 4c). Typically, the result from the RFM2 forced with MH3 rainfall points to 16.5% of wetland fraction in North Africa. However, large areas of wetlands and lakes have disappeared because of natural climate change during the past 6 kyr (Kropelin et al., 2008) and anthropogenic impact after the industrial revolution (Hu, Niu, Chen, Li et al., 2017). According to estimates averaging over all TCI and RFM, climate change from mid-Holocene (MH3) to PI period leads to a wetland loss by 7.8% land areas of North Africa (Figure 4c). The drop of wetland area was more prominent in regions north of 10°N by 10.4%. Subsequently, wetlands north of 10°N decreased from 7.7% in PI period to a present potential value of 6.4% (Figure 4c), higher than the observation of 0.8% (Gumbricht et al., 2017) which may neglect very small-scale endorheic wetlands and result from direct human modifications.

The status of individual hydrological elements during the mid-Holocene was characterized through the study of shoreline sediments, lacustrine deposits, aquatic fossils, satellite images, and topographic data (Drake et al., 2011; Kohfeld & Harrison, 2000; Lézine et al., 2011), but the associated rainfall is controversial (Engel et al., 2017; Quade et al., 2018). The relationship between wetland fraction and precipitation was thus examined in our wetland models. For RFM2, paleolakes in the mid-Holocene Sahara could be sustained only if the annual precipitation is at least 700 mm/yr, corresponding to the 25th percentile of annual precipitation for 0.1° grid-cells with a wetland fraction of 50%–100% (Figure 4b). To form a wetland fraction larger than 10% for 0.1° grid-cells, at least 480 mm/yr of precipitation is required, which is consistent with the estimate of ~400 mm/yr from pollen data and vegetation simulations (Bartlein et al., 2010; Chen et al., 2020). Previous vegetation reconstructions of the Green Sahara were either at coarse spatial resolution of 1°–3° through modeling (Hopcroft et al., 2017; Lu et al., 2018; Pausata et al., 2020), or at site scale using pollen records. It is possible that vegetation patches were only prevailing along river networks and

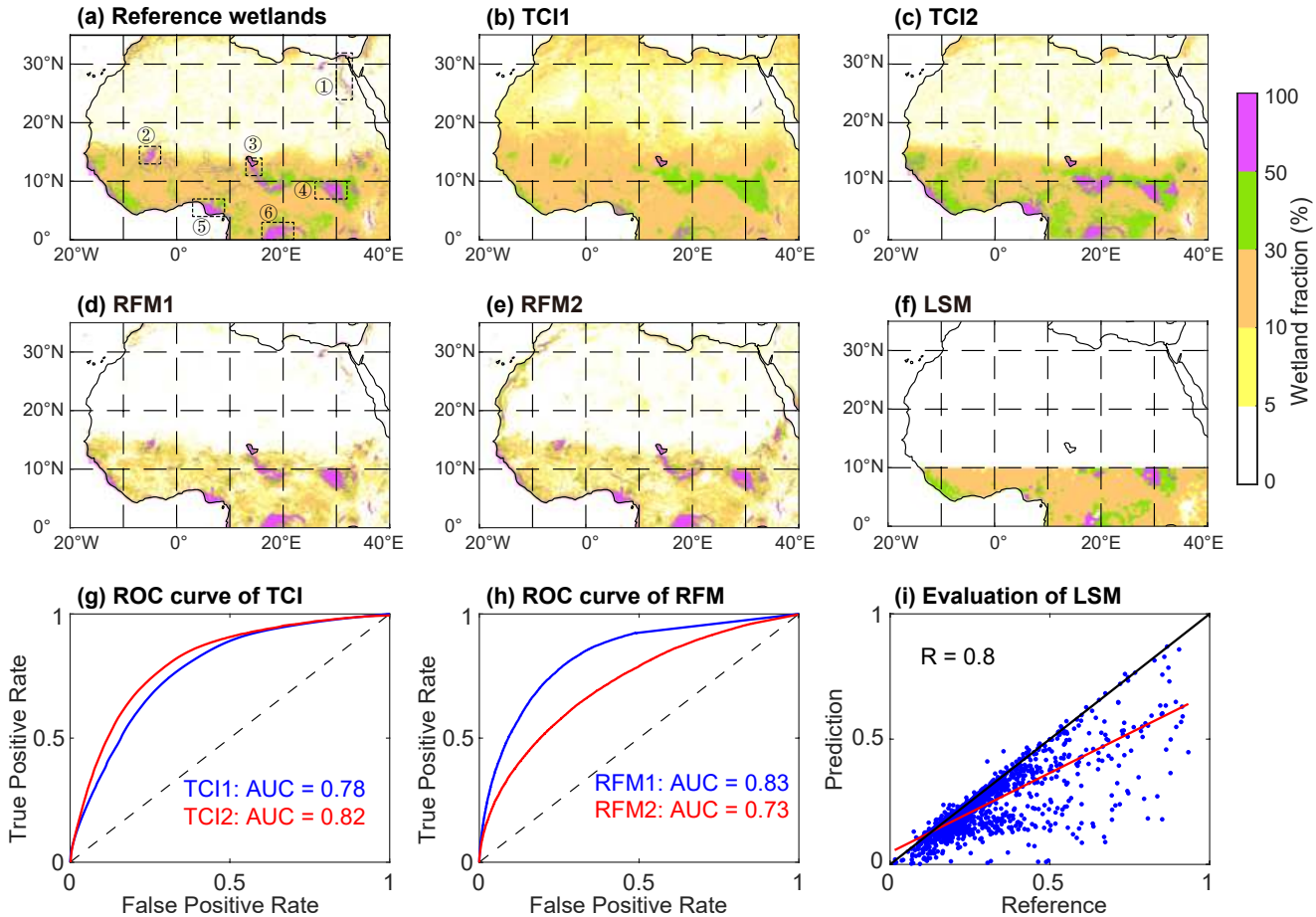

Figure 2. Performance of the five wetland models. (a) Present reference wetland map from Tootchi et al. (2019), upscaled from 15″ to 0.1°. The dashed rectangle demotes the six dense wetland complexes: C1-Nile Delta, C2-Middle Niger River Basin, C3-Lake Chad, C4-South Sudan, C5-Niger River Delta, and C6-Cuvette Centrale. (b–f) The reproduced present wetlands from models and (g)–(i) the comparison with reference map.

near wetlands where soil water was sufficient to support semiarid ecosystems. Therefore, improved rainfall estimates for lakes and wetlands could better characterize spatial pattern of vegetation and climate in the mid-Holocene Sahara.

This work applied multiple methods to narrow the uncertainties of reconstructed wetland areas for the mid-Holocene North Africa. Each model has its advantage and uncertainties. The TCI approach uses the least predictors and has efficient performance in regions where wetland development is determined by precipitation and topography information. However, it is difficult to improve this approach constrained by the TCI definitions and equations. The RFM approach is purely diagnostic but flexible and could include more relevant predictors depending on available data. In addition, the RFM can rank the relative importance of predictor variables. It produced the most plausible result in this work, possibly because it was trained with many calibrated data at high spatial resolution. The LSM approach considers more boundary conditions and accounts for physical processes but currently the lack of available paleo-data for improving the LSM limits its performance compared to purely diagnostic models, for example, paleoclimate data and vegetation types and parameters (rooting depth) should ameliorate the simulation of the mean water table over large grid cells with LSMs. Thus, process-based LSMs may have more potential in future work. Future attempts to reduce uncertainties of the result may consider factors like soil texture and use a more realistic climate forcing besides rainfall.

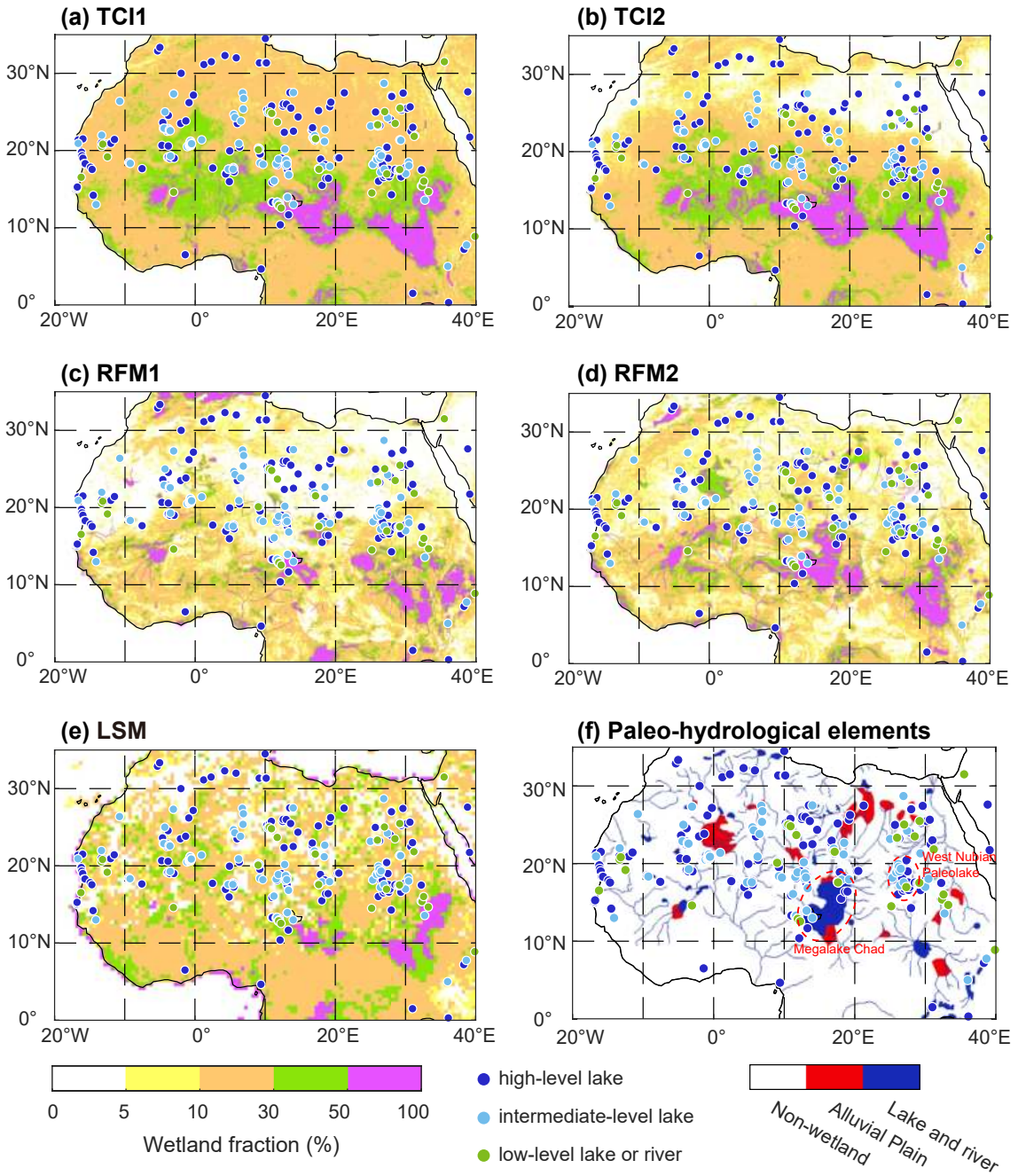

Figure 3. Reconstructed wetlands and paleo-hydrological records over mid-Holocene North Africa. (a–e) Mid-Holocene wetland fraction from the five wetland models with MH3. (f) Paleo-hydrological elements revised from Drake et al. (2011) and Larrasoana et al. (2013). Colored dots in each panel denote the 297 paleolake records during 8–5 ka from Kohfeld and Harrison (2000) and Lézine et al. (2014).

5. Conclusion

In this study, we present reconstructions of wetland distribution in the mid-Holocene North Africa using five calibrated wetland models and four precipitation levels. Results show that TCI2 and RFM1 have the best ability to reproduce present wetlands while simulations from RFM2 are in better agreement with paleo-hydrological records. Therefore, the result from RFM2 under MH3 climate might be the most realistic wetland map for the mid-Holocene North Africa. Our simulation indicates that, at least 480 mm/yr of mid-Holocene annual precipitation is required to sustain a wetland fraction larger than 10% at 0.1° grid-cell

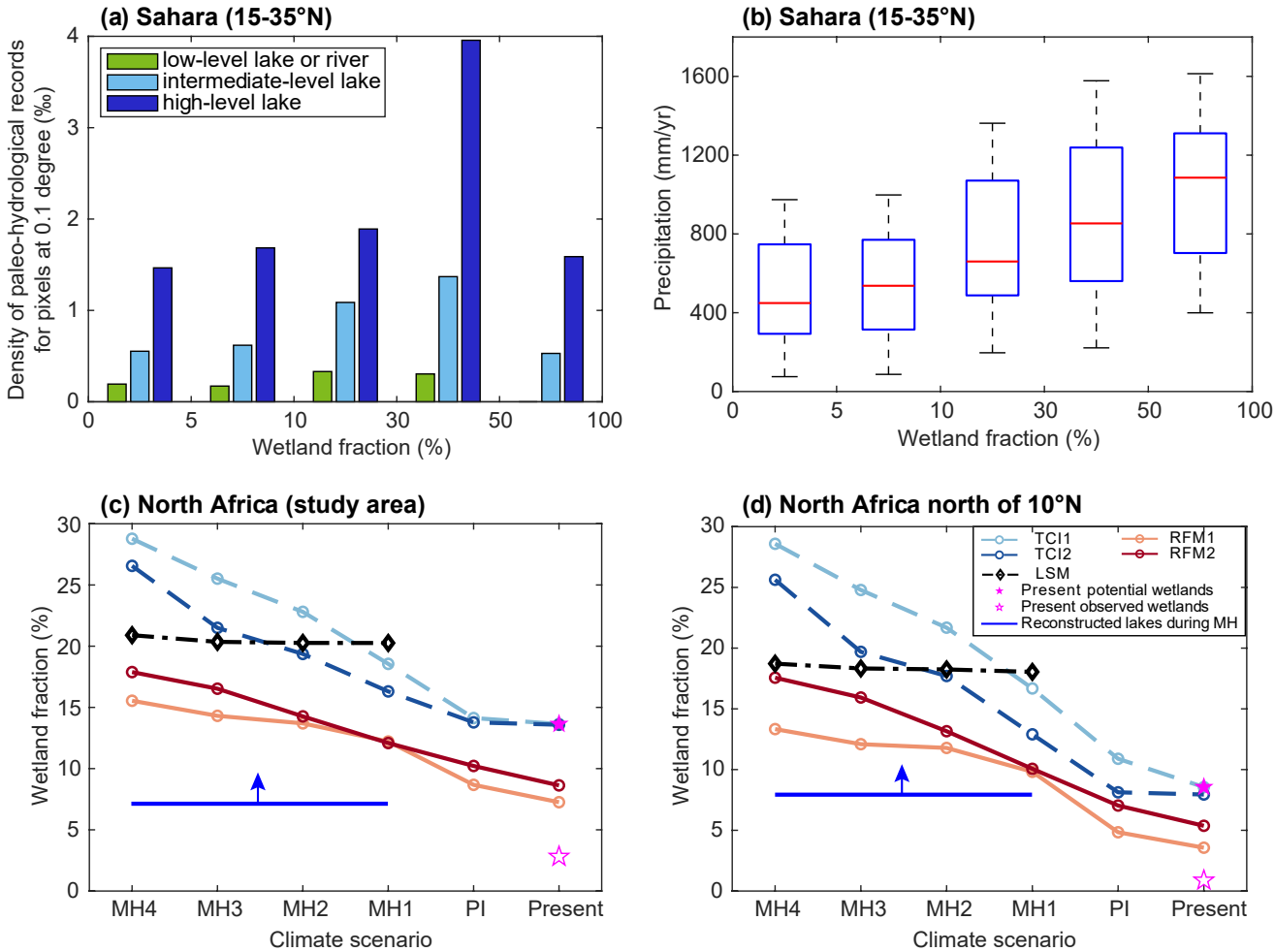

Figure 4. Simulated wetland fraction for different climate scenarios and relationships with precipitation and paleo-records. (a) Density of paleolake records (Kohfeld & Harrison, 2000; Lézine et al., 2014) as a function of reconstructed wetland fraction intervals from RFM2 simulation with MH3 (Figure 3d). (b) Relationship between precipitation and produced wetland fractions in Sahara from RFM2 simulation with MH3; Lower and upper edges of blue box and red lines indicate 25th and 75th percentiles and median of precipitation, respectively. Other models are shown in Figures S7 in Supporting Information S1. (c and d) Total wetland fraction from mid-Holocene (MH) and pre-industrial (PI) period to present; the present potential wetland fraction is derived from Tootchi et al. (2019) (Figure 2a); the present observed wetland fraction is estimated based on Gumbricht et al. (2017); the total lake fraction is calculated based on Figure 3f.

scale over the Sahara (15°–35°N). During the mid-Holocene, 18.9 ± 4.0% of land surface in North Africa was covered by wetlands. From the mid-Holocene to PI period, wetland areas decreased by 7.8% of North African land surface. Our newly developed reconstructions provide a basis to include wetland feedbacks on vegetation and climate with further land surface and climate modeling.

Data Availability Statement

The produced wetland maps from the 20 mid-Holocene simulations are available at Mendeley Data (http://dx.doi.org/10.17632/8vfhhv8s2f.1). The authors appreciate Anne-Marie Lézine and Juan C. Larrasoana for sharing the compiled data of paleo-hydrological elements and paleolake status during the mid-Holocene.

Acknowledgments
This study was supported by the Fundamental Research Funds for the Central Universities, the China University of Geosciences (Wuhan) (No. CUG2106323), the China Postdoctoral Science Foundation (No. 2021M692976), the National Natural Science Foundation of China (No. 41772029), and the 111 Project (No. BP0820004).

References

Armstrong, E., Hopcroft, P. O., & Valdes, P. J. (2019). A simulated Northern Hemisphere terrestrial climate dataset for the past 60,000 years. *Scientific Data*, *6*(1), 265. https://doi.org/10.1038/s41597-019-0277-1

Bartlein, P. J., Harrison, S. P., Brewer, S., Connor, S., Davis, B. A. S., Gajewski, K., et al. (2010). Pollen-based continental climate reconstructions at 6 and 21 ka: A global synthesis. *Climate Dynamics*, *37*(3–4), 775–802. https://doi.org/10.1007/s00382-010-0904-1

Beven, K. J., & Kirkby, M. J. (1979). A physically based, variable contributing area model of basin hydrology/Un modèle à base physique de zone d'appel variable de l'hydrologie du bassin versant. *Hydrological Sciences Bulletin*, *24*(1), 43–69. https://doi.org/10.1080/02626667909491834

Beyer, R. M., Krapp, M., & Manica, A. (2020). High-resolution terrestrial climate, bioclimate and vegetation for the last 120,000 years. *Scientific Data*, *7*(1), 236. https://doi.org/10.1038/s41597-020-0552-1

Boucher, O., Servonnat, J., Albright, A. L., Aumont, O., Balkanski, Y., Bastrikov, V., et al. (2020). Presentation and evaluation of the IPSL-CM6A-LR Climate Model. *Journal of Advances in Modeling Earth Systems*, *12*(7), e2019MS002010.

Braconnot, P., Albani, S., Balkanski, Y., Cozic, A., Kageyama, M., Sima, A., et al. (2021). Impact of dust in PMIP-CMIP6 mid-Holocene simulations with the IPSL model. *Climate of the Past*, *17*(3), 1091–1117. https://doi.org/10.5194/cp-17-1091-2021

Breiman, L. (2001). Random forests. *Machine Learning*, *45*(1), 5–32. https://doi.org/10.1023/a:1010933404324

Brierley, C. M., Zhao, A. N., Harrison, S. P., Braconnot, P., Williams, C. J. R., Thornalley, D. J. R., et al. (2020). Large-scale features and evaluation of the PMIP4-CMIP6 midHolocene simulations. *Climate of the Past*, *16*(5), 1847–1872. https://doi.org/10.5194/cp-16-1847-2020

Chandan, D., & Peltier, W. R. (2020). African humid period precipitation sustained by robust vegetation, soil, and lake feedbacks. *Geophysical Research Letters*, *47*(21), e2020GL088728. https://doi.org/10.1029/2020gl088728

Chen, W. Z., Ciais, P., Zhu, D., Ducharne, A., Viovy, N., Qiu, C. J., & Huang, C. (2020). Feedbacks of soil properties on vegetation during the Green Sahara period. *Quaternary Science Reviews*, *240*, 106389. https://doi.org/10.1016/j.quascirev.2020.106389

Claussen, M., & Gayler, V. (1997). The greening of the Sahara during the mid-Holocene: Results of an Interactive Atmosphere-Biome Model. *Global Ecology and Biogeography Letters*, *6*(5), 369–377. https://doi.org/10.2307/2997337

Curie, F., Gaillard, S., Ducharne, A., & Bendjoudi, H. (2007). Geomorphological methods to characterise wetlands at the scale of the Seine watershed. *The Science of the Total Environment*, *375*(1–3), 59–68. https://doi.org/10.1016/j.scitotenv.2006.12.013

Cutler, D. R., Edwards, T. C., Jr., Beard, K. H., Cutler, A., Hess, K. T., Gibson, J., & Lawler, J. J. (2007). Random forests for classification in ecology. *Ecology*, *88*(11), 2783–2792. https://doi.org/10.1890/07-0539.1

Drake, N. A., Blench, R. M., Armitage, S. J., Bristow, C. S., & White, K. H. (2011). Ancient watercourses and biogeography of the Sahara explain the peopling of the desert. *Proceedings of the National Academy of Sciences of the United States of America*, *108*(2), 458–462. https://doi.org/10.1073/pnas.1012231108

Engel, M., Matter, A., Parker, A. G., Parton, A., Petraglia, M. D., Preston, G. W., & Preusser, F. (2017). Lakes or wetlands? A comment on 'The middle Holocene climatic records from Arabia: Reassessing lacustrine environments, shift of ITCZ in Arabian Sea, and impacts of the southwest Indian and African monsoons' by Enzel et al. *Global and Planetary Change*, *148*, 258–267. https://doi.org/10.1016/j.gloplacha.2016.11.001

Felton, B. R., O'Neil, G. L., Robertson, M. M., Fitch, G. M., & Goodall, J. L. (2019). Using random forest classification and nationally available geospatial data to screen for wetlands over large geographic regions. *Water*, *11*(6), 1158. https://doi.org/10.3390/w11061158

Fick, S. E., & Hijmans, R. J. (2017). WorldClim 2: New 1-km spatial resolution climate surfaces for global land areas. *International Journal of Climatology*, *37*(12), 4302–4315. https://doi.org/10.1002/joc.5086

GRDC. (2020). *Major river basins of the World/Global Runoff Data Centre, GRDC. 2nd, rev. ext*. Federal Institute of Hydrology (BfG).

Gumbricht, T., Roman-Cuesta, R. M., Verchot, L., Herold, M., Wittmann, F., Householder, E., et al. (2017). An expert system model for mapping tropical wetlands and peatlands reveals South America as the largest contributor. *Global Change Biology*, *23*(9), 3581–3599. https://doi.org/10.1111/gcb.13689

Harrison, S. P., Bartlein, P. J., Izumi, K., Li, G., Annan, J., Hargreaves, J., et al. (2015). Evaluation of CMIP5 palaeo-simulations to improve climate projections. *Nature Climate Change*, *5*(8), 735–743. https://doi.org/10.1038/nclimate2649

Hijmans, R. J., Cameron, S. E., Parra, J. L., Jones, P. G., & Jarvis, A. (2005). Very high resolution interpolated climate surfaces for global land areas. *International Journal of Climatology*, *25*(15), 1965–1978. https://doi.org/10.1002/joc.1276

Hoelzmann, P., Jolly, D., Harrison, S. P., Laarif, F., Bonnefille, R., & Pachur, H. J. (1998). Mid-Holocene land-surface conditions in northern Africa and the Arabian Peninsula: A data set for the analysis of biogeophysical feedbacks in the climate system. *Global Biogeochemical Cycles*, *12*(1), 35–51. https://doi.org/10.1029/97gb02733

Hoelzmann, P., Kruse, H. J., & Rottinger, F. (2000). Precipitation estimates for the eastern Saharan palaeomonsoon based on a water balance model of the West Nubian Palaeolake Basin. *Global and Planetary Change*, *26*(1–3), 105–120. https://doi.org/10.1016/s0921-8181(00)00038-2

Hopcroft, P. O., Valdes, P. J., Harper, A. B., & Beerling, D. J. (2017). Multi vegetation model evaluation of the Green Sahara climate regime. *Geophysical Research Letters*, *44*(13), 6804–6813. https://doi.org/10.1002/2017gl073740

Hu, S. J., Niu, Z., Chen, Y., Li, L., & Zhang, H. (2017). Global wetlands: Potential distribution, wetland loss, and status. *The Science of the Total Environment*, *586*, 319–327. https://doi.org/10.1016/j.scitotenv.2017.02.001

Hu, S. J., Niu, Z. G., & Chen, Y. F. (2017). Global wetland datasets: A Review. *Wetlands*, *37*(5), 807–817. https://doi.org/10.1007/s13157-017-0927-z

Kohfeld, K. E., & Harrison, S. P. (2000). How well can we simulate past climates? Evaluating the models using global palaeoenvironmental datasets. *Quaternary Science Reviews*, *19*(1–5), 321–346. https://doi.org/10.1016/s0277-3791(99)00068-2

Krinner, G., Lézine, A. M., Braconnot, P., Sepulchre, P., Ramstein, G., Grenier, C., et al. (2012). A reassessment of lake and wetland feedbacks on the North African Holocene climate. *Geophysical Research Letters*, *39*(7), L07701. https://doi.org/10.1029/2012gl050992

Kropelin, S., Verschuren, D., Lézine, A. M., Eggermont, H., Cocquyt, C., Francus, P., et al. (2008). Climate-driven ecosystem succession in the Sahara: The past 6000 years. *Science*, *320*(5877), 765–768.

Kutzbach, J. E. (1981). Monsoon climate of the Early Holocene: Climate experiment with the Earth's orbital parameters for 9000 years ago. *Science*, *214*(4516), 59–61. https://doi.org/10.1126/science.214.4516.59

Larrasoana, J. C., Roberts, A. P., & Rohling, E. J. (2013). Dynamics of green Sahara periods and their role in hominin evolution. *PLOS One*, *8*(10), e76514. https://doi.org/10.1371/journal.pone.0076514

Lehner, B., & Grill, G. (2013). Global river hydrography and network routing: Baseline data and new approaches to study the world's large river systems. *Hydrological Processes*, *27*(15), 2171–2186. https://doi.org/10.1002/hyp.9740

Lézine, A.-M., Bassinot, F., & Peterschmitt, J.-Y. (2014). Orbitally-induced changes of the Atlantic and Indian monsoons over the past 20,000 years: New insights based on the comparison of continental and marine records. *Bulletin de la Societe Geologique de France*, *185*(1), 3–12. https://doi.org/10.2113/gssgfbull.185.1.3

Lézine, A.-M., Hély, C., Grenier, C., Braconnot, P., & Krinner, G. (2011). Sahara and Sahel vulnerability to climate changes, lessons from Holocene hydrological data. *Quaternary Science Reviews*, *30*(21–22), 3001–3012. https://doi.org/10.1016/j.quascirev.2011.07.006

Lu, Z., Miller, P. A., Zhang, Q., Zhang, Q., Wårlind, D., Nieradzik, L., et al. (2018). Dynamic vegetation simulations of the mid-Holocene Green Sahara. *Geophysical Research Letters*, *45*(16), 8294–8303. https://doi.org/10.1029/2018gl079195

Marthews, T. R., Dadson, S. J., Lehner, B., Abele, S., & Gedney, N. (2015). High-resolution global topographic index values for use in large-scale hydrological modelling. *Hydrology and Earth System Sciences*, *19*(1), 91–104. https://doi.org/10.5194/hess-19-91-2015

Merot, P., Squividant, H., Aurousseau, P., Hefting, M., Burt, T., Maitre, V., et al. (2003). Testing a climato-topographic index for predicting wetlands distribution along an European climate gradient. *Ecological Modelling*, *163*(1–2), 51–71. https://doi.org/10.1016/s0304-3800(02)00387-3

Molnar, P., & Rajagopalan, B. (2020). Mid-Holocene Sahara-Sahel precipitation from the vantage of present-day climate. *Geophysical Research Letters*, *47*(16), e2020GL088171. https://doi.org/10.1029/2020gl088171

O'ishi, R., & Abe-Ouchi, A. (2013). Influence of dynamic vegetation on climate change and terrestrial carbon storage in the Last Glacial Maximum. *Climate of the Past*, *9*(4), 1571–1587. https://doi.org/10.5194/cp-9-1571-2013

Palchan, D., & Torfstein, A. (2019). A drop in Sahara dust fluxes records the northern limits of the African Humid Period. *Nature Communications*, *10*(1), 3803. https://doi.org/10.1038/s41467-019-11701-z

Pausata, F. S. R., Gaetani, M., Messori, G., Berg, A., Maia de Souza, D., Sage, R. F., & deMenocal, P. B. (2020). The greening of the Sahara: Past changes and future implications. *One Earth*, *2*(3), 235–250. https://doi.org/10.1016/j.oneear.2020.03.002

Qiu, C. J., Zhu, D., Ciais, P., Guenet, B., Peng, S. S., Krinner, G., et al. (2019). Modelling northern peatland area and carbon dynamics since the Holocene with the ORCHIDEE-PEAT land surface model (SVN r5488). *Geoscientific Model Development*, *12*(7), 2961–2982. https://doi.org/10.5194/gmd-12-2961-2019

Quade, J., Dente, E., Armon, M., Ben Dor, Y., Morin, E., Adam, O., & Enzel, Y. (2018). Megalakes in the Sahara? A review. *Quaternary Research*, *90*(2), 253–275. https://doi.org/10.1017/qua.2018.46

Skonieczny, C., Paillou, P., Bory, A., Bayon, G., Biscara, L., Crosta, X., et al. (2015). African humid periods triggered the reactivation of a large river system in Western Sahara. *Nature Communications*, *6*, 8751. https://doi.org/10.1038/ncomms9751

Stocker, B. D., Spahni, R., & Joos, F. (2014). DYPTOP: A cost-efficient TOPMODEL implementation to simulate sub-grid spatio-temporal dynamics of global wetlands and peatlands. *Geoscientific Model Development*, *7*(6), 3089–3110. https://doi.org/10.5194/gmd-7-3089-2014

Sun, W. Y., Wang, B., Zhang, Q., Pausata, F. S. R., Chen, D. L., Lu, G. N., et al. (2019). Northern Hemisphere land monsoon precipitation increased by the Green Sahara during middle Holocene. *Geophysical Research Letters*, *46*(16), 9870–9879. https://doi.org/10.1029/2019gl082116

Swets, J. A. (1988). Measuring the accuracy of diagnostic systems. *Science*, *240*(4857), 1285–1293. https://doi.org/10.1126/science.3287615

Texier, D., de Noblet, N., & Braconnot, P. (2000). Sensitivity of the African and Asian monsoons to mid-Holocene insolation and data-inferred surface changes. *Journal of Climate*, *13*(1), 164–181. https://doi.org/10.1175/1520-0442(2000)013<0164:sotaaa>2.0.co;2

Tian, F., Cao, X. Y., Dallmeyer, A., Zhao, Y., Ni, J., & Herzschuh, U. (2017). Pollen-climate relationships in time (9 ka, 6 ka, 0 ka) and space (upland vs. lowland) in eastern continental Asia. *Quaternary Science Reviews*, *156*, 1–11. https://doi.org/10.1016/j.quascirev.2016.11.027

Tierney, J. E., Pausata, F. S., & de Menocal, P. B. (2017). Rainfall regimes of the Green Sahara. *Science Advances*, *3*(1), e1601503. https://doi.org/10.1126/sciadv.1601503

Tootchi, A., Jost, A., & Ducharne, A. (2019). Multi-source global wetland maps combining surface water imagery and groundwater constraints. *Earth System Science Data*, *11*(1), 189–220. https://doi.org/10.5194/essd-11-189-2019

Wei, Y., Liu, S., Huntzinger, D. N., Michalak, A. M., Viovy, N., Post, W. M., et al. (2014). The North American Carbon Program Multi-scale Synthesis and Terrestrial Model Intercomparison Project – Part 2: Environmental driver data. *Geoscientific Model Development*, *7*(6), 2875–2893. https://doi.org/10.5194/gmd-7-2875-2014

Xue, Z. S., Zou, Y. C., Zhang, Z. S., Lyu, X. G., Jiang, M., Wu, H. T., et al. (2018). Reconstruction and future prediction of the distribution of wetlands in China. *Earths Future*, *6*(11), 1508–1517. https://doi.org/10.1029/2017ef000807